

Personalized Modeling of Atrial Activation and P-waves: a Comparison Between Invasive and Non-invasive Cardiac Mapping

Patricia Martínez Díaz¹, Jorge Sánchez^{1,2}, Claudia Nagel¹, Marta Martínez Pérez²,
Ismael Hernández Romero², María S Guillem², Olaf Dössel¹ and Axel Loewe¹

¹ Institute of Biomedical Engineering, Karlsruhe Institute of Technology (KIT), Karlsruhe, Germany

² Institute of Information and Communication Technologies, Universitat Politècnica de València (UPV), Valencia, Spain

Abstract

Biatrial personalized models incorporating functional and anatomical features are becoming a promising tool for planning therapy for patients with atrial fibrillation (AF). Conduction velocity (CV) is one of the main features to be matched during the process of functional personalization, as it can identify electrical abnormalities in the cardiac tissue. The spatial distribution of CV can be estimated from local activation times (LAT) maps from non-invasive electrocardiographic imaging (ECGI) or invasive electroanatomical mapping systems (EAMS). We investigated the effect of using either invasive LAT maps from EAMS or non-invasive LAT maps from ECGI to personalize two biatrial models by comparing the virtual P-waves obtained from these LAT maps with the measured P-waves from the surface electrocardiogram (ECG). For both modalities – ECGI and EAMS – we found a qualitative match between simulated and measured P-waves but observed quantitative differences. The root-mean-square error (RMSE) between measured and simulated signals for patient A was 0.26 ± 0.11 mV and 0.38 ± 0.31 mV, while for patient B it was 0.21 ± 0.09 mV and 0.14 ± 0.05 mV for EAMS and ECGI, respectively. The correlation between measured and simulated signals from ECGI and EAMS was 0.69 ± 0.34 and 0.71 ± 0.26 for patient A and 0.71 ± 0.18 and 0.72 ± 0.18 for patient B. Our results suggest that LAT maps from ECGI and EAMS show differences, which are also reflected in the computed P-wave on the body surface.

1. Introduction

Personalized atrial models including anatomical and functional features have been used as mechanistic tools to understand the dynamics of atrial fibrillation (AF) and to predict therapy success [1]. One of the principal features of interest in the process of functional twinning

is the incorporation of conduction velocity (CV) information into the personalized model. CV is an electrophysiological (EP) property that describes the direction-dependent (anisotropic) and spatially heterogeneous speed with which the electrical depolarization wave spreads in the cardiac tissue [2]. Changes in CV can be associated with the location of the underlying arrhythmogenic substrate [3]. When creating a patient-specific digital model for therapy planning, it is therefore important to match this parameter to represent the electrical propagation accurately. Mean CV can be estimated from P-wave duration from the body surface electrocardiogram (ECG) [4]. Regional CV can be calculated from local activation times (LAT) maps obtained from non-invasive electrocardiographic imaging (ECGI) [5] or from invasive intracardiac electrograms (IEGM) [2, 6] from electroanatomical mapping systems (EAMS). LAT maps from EAMS have usually higher resolution and provide a more accurate representation of the electrical propagation as the catheter is placed closer to the cardiac source [7]. On the other hand, ECGI has the advantage of reconstructing atrial activation from torso recordings, eliminating the risk of an invasive procedure.

Several research groups have described processes to create personalized atrial models, these include the use of only pre-procedural information such as magnetic resonance imaging (MRI) and computed tomography scans (CT) [8,9], or the use of procedural data together with non-invasive imaging techniques [1, 10, 11]. However, it remains unclear whether using non-invasive pre-procedural data is sufficient when creating personalized atrial models for therapy planning or if further activation data is required from invasive recordings [12]. Our method generated synthetic P-waves using LAT maps from invasive and non-invasive data. We studied the influence of the selected input data modality on the morphology of the computed P-waves and we finally compared them with the P-waves measured on the surface of the torso.

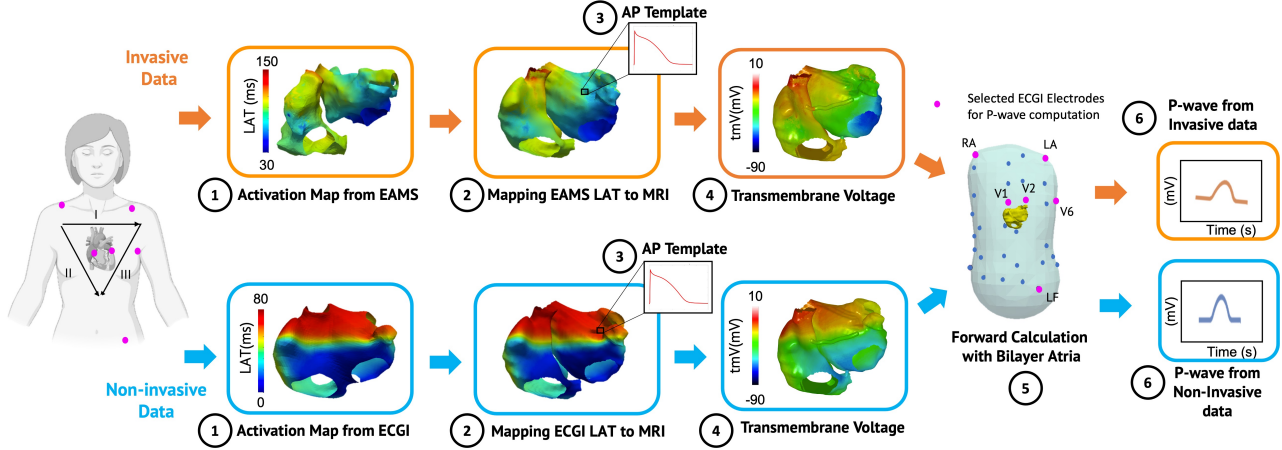


Figure 1. Study pipeline: LAT data were mapped to the MRI geometry and interpolated. A precomputed atrial action potential (AP) was placed in every node of the bilayer model and shifted in time according to the LAT. Extracellular potentials were recovered at selected electrode positions on the torso surface to obtain virtual P-waves.

2. Methods

Data from the invasive Carto® 3 EAMS (Biosense Webster), from the non-invasive ECGI system Acorys® (Corify Care), and biatrial geometries from a 3-Tesla CMR scanner (Siemens Healthcare) segmented using ADAS® software (Galgo Medical) were obtained from two patients at Hospital Clínic, Barcelona undergoing catheter ablation of AF (Patient A: female, 61 years with persistent AF and patient B: male 58 years with paroxysmal AF). Both patients are part of the NOISE-AF study (NCT04496336), provided written informed consent and the protocol was approved by the hospital ethics committee. Invasive and non-invasive LAT maps before ablation were obtained during sinus rhythm for patient A and during coronary sinus pacing for patient B. A summary of the study pipeline is presented in Figure 1.

2.1. Electrocardiographic Imaging Data

The electrical activation of the atria was reconstructed by solving the inverse electrocardiography problem from body surface potential recordings. The torso surface was reconstructed from a 360° video of the patient’s chest while wearing the 64-electrode vest. The biatrial geometries from ECGI consisted of a shell of the MRI segmentation having both atria fused. The ECGI shell was already aligned to the original MRI geometry, so no additional co-registration step was needed. To compare the measured P-waves to our computed P-waves, 6 electrodes from ECGI resembling standard ECG locations were used to obtain 9-lead reference traces (I, II, III, aVR, aVL, aVF, V1, V2 and V6).

2.2. Electroanatomical Mapping Data

Endocardial biatrial geometries and LAT maps were generated from the CARTO® 3 cases using IEGM recordings. The activation sequence was verified to disregard LAT artifacts by leveraging a priori knowledge about the expanding wavefront [13]. We divided the set P of points x in the LAT map into N activation bands Γ_i starting at the earliest activation point x_{EAP} up to the latest activation point x_{LAP} , with a temporal resolution $dt = 5$ ms:

$$\Gamma_i = \{x \in P \mid \text{LAT}(x_{EAP}) + dt \cdot i < \text{LAT}(x) \leq \text{LAT}(x_{EAP}) + dt \cdot (i + 1)\} \quad (1)$$

To disregard outliers, x_{EAP} was defined as the center of mass of the region below the 2.5th percentile of the LAT distribution and x_{LAP} of those above the 97.5th percentile. The biggest connected island within the 2.5th percentile of the LAT was used to initialize the first reliable region X_0 . The domain of each band Γ_i contains M_i islands of points x to be classified as reliable or artifact annotations. Islands are classified as reliable and added to the region C if a maximum distance between the centroid of the current reliable region X_i and the centroid of the island $X_{i,j}$ is fulfilled:

$$\|C(X_i) - C(X_{i,j})\| \leq 1 + i, \text{ mm} \quad (2)$$

X_i is then initialized with X_{i-1} and a new centroid is calculated in the next iteration. The final LAT map consisted only of reliable regions and was then mapped to the MRI geometry. For image co-registration, the veins and valves were manually clipped using Paraview v5.9.1 (Kitware). Then the centroids of the valve and vein rings were

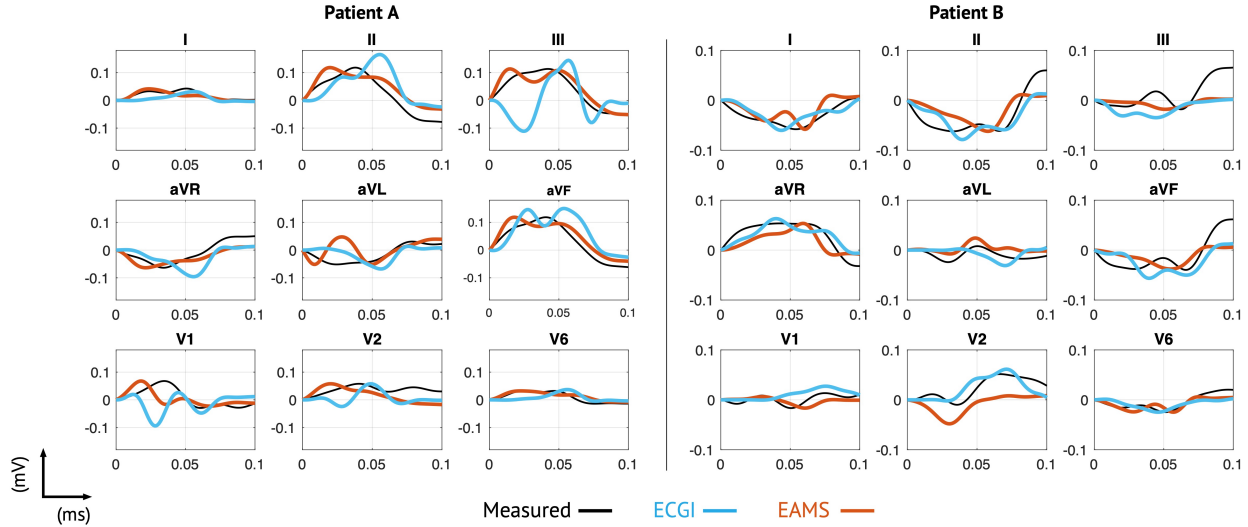


Figure 2. Comparison between computed and measured P-waves: Patient A data was obtained during coronary sinus pacing while Patient B data was obtained during sinus rhythm. Measured P-waves are shown in black, the P-waves computed based on EAMS LAT maps are colored in orange, and the P-waves from ECGI LAT data are colored in blue. The signals were aligned and amplified to match the amplitude of the measured P-wave for each lead.

extracted and used as landmarks to perform rigid alignment of the EAMS geometry to the biatrial MRI. The iterative closest point algorithm was used to further co-register the clipped biatrial endocardial geometry to the MRI geometry with Scalismo®.

2.3. P-wave Forward Computation

Each LAT map was transferred to the MRI geometry using nearest neighbor projection and Laplacian interpolation was performed to fill the gaps in the data distribution. A bilayer model was generated for each patient from the MRI data [13]. LAT maps from ECGI and EAMS on the MRI surface were used to shift a pre-computed atrial action potential template in time for each of the nodes in the bilayer model, respectively. For the forward calculation of virtual P-waves, extracellular potentials on the body surface were recovered using openCARP [14] from the same 6 previously selected electrode locations. The atria were assumed to be immersed in an infinite volume conductor [15]. Simulated P-waves were low-pass filtered with a cutoff frequency of 40 Hz and then individually amplified to match the maximum amplitude of their corresponding measured P-wave per lead. The two sets of virtual P-waves were aligned to the corresponding measured P-wave using cross-correlation and the root-mean-square error (RMSE) was calculated for the whole set.

3. Results

Virtual P-waves obtained from ECGI and EAMS LAT maps were compared to the measured P-waves as shown in Figure 2. For the computed P-waves based on the LAT maps derived from both modalities - ECGI and EAMS, the morphology matches the simulated P-waves qualitatively. However, quantitative differences exist. The RMSE was measured for each lead for the whole atrial activation time defined by the P-wave duration on the surface ECG and then averaged among all leads. Values are presented as mean and standard deviation across all 9 leads. In general, the polarity of virtual signals in lead II coincides with the expected direction of the P-wave, meaning that lead II is positive during sinus rhythm and negative during pacing from the coronary sinus. P-waves computed based on ECGI LAT maps show a reduced P-wave duration as seen in the non-invasive LAT map. P-waves computed based on EAMS LAT maps have a similar duration to the measured P-wave on the body surface.

Table 1. Root-mean-square error (RMSE) and correlation between measured P-wave and simulated P-wave. Values are presented as mean and standard deviation across all 9 leads.

Patient	LAT data	RMSE (mV)	Correlation
A	ECGI	0.26 ± 0.11	0.69 ± 0.34
	EAMS	0.38 ± 0.31	0.71 ± 0.26
B	ECGI	0.21 ± 0.09	0.71 ± 0.18
	EAMS	0.14 ± 0.05	0.72 ± 0.18

4. Discussion

The aim of this work was to compare the differences in computing P-waves derived from invasive EAMS and non-invasive ECGI LAT maps. For both patients, ECGI LAT maps had a total activation time shorter than the total duration of the surface P-wave, therefore the P-wave duration of synthetic signals was also shortened. This can be explained because the slew rate of P-waves is usually slower than the one of the IEGM. In addition, noisy recordings and baseline fluctuations can also affect the ECGI LAT activation threshold. Another cause that may explain the reduction of the ECGI P-wave duration is the loss of information in the septum, which causes the right atrium and left atrium to be activated almost simultaneously.

We assigned the same activation in the endocardial and epicardial layers, this means that the activation was modeled as transmurally homogeneous [16]. Future work could examine the influence of incorporating transmural conduction delay or fibrosis information to personalize our bilayer model. In addition, the impact of the chosen clinical data on the arrhythmia vulnerability of the model can be further tested by using established pacing protocols [17].

We computed P-waves from clinically measured invasive and non-invasive LAT maps and showed that the selection of input data affects the activation pattern and that the differences between ECGI and EAMS LAT maps are also reflected in the computed P-wave on the body surface.

Acknowledgments

This project has received funding from the European Union's Horizon 2020 research and innovation programme under the Marie Skłodowska-Curie grant agreement No 860974.

References

- [1] Azzolin L, Eichenlaub M, Nagel C, Nairn D, et al. Personalized ablation vs. conventional ablation strategies to terminate atrial fibrillation and prevent recurrence. *EP Europace* 2022;doi:10.1093/europace/eaac116.
- [2] Coveney S, Cantwell C, Roney C. Atrial conduction velocity mapping: clinical tools, algorithms and approaches for understanding the arrhythmogenic substrate. *Med Biol Eng Comput* 2022;60:2463–2478.
- [3] Nairn D, Eichenlaub M, Müller Edenborn B, et al. LGE-MRI for diagnosis of left atrial cardiomyopathy as identified in high-definition endocardial voltage and conduction velocity mapping. *medRxiv* 2022; doi:10.1101/2022.02.02.22269817.
- [4] Krueger MW, Seemann G, Rhode K, et al. Personalization of atrial anatomy and electrophysiology as a basis for clinical modeling of radio-frequency ablation of atrial fibrillation. *IEEE Trans Med Imaging* 2013;32(1):73–84.
- [5] Salinet J, Molero R, Schlindwein FS, Karel J, et al. Electrocardiographic imaging for atrial fibrillation: a perspective from computer models and animal experiments to clinical value. *Front Physiol* 2021;12.
- [6] Verma B, Oesterlein T, Loewe A, et al. Regional conduction velocity calculation from clinical multichannel electrograms in human atria. *Comp Biol Med* 2018;92:188–196.
- [7] Graham AJ, Orini M, Zacur E, Dhillon G, et al. Simultaneous comparison of electrocardiographic imaging and epicardial contact mapping in structural heart disease. *Circ Arrhythm Electrophysiol* 4 2019;12(4):e007120.
- [8] Boyle PM, Zghaib T, Zahid S, Ali RL, et al. Computationally guided personalized targeted ablation of persistent atrial fibrillation. *Nat Biomed Eng* 2019;3(11):870–879.
- [9] Shade JK, Ali RL, Basile D, Popescu D, et al. Pre-procedure application of machine learning and mechanistic simulations predicts likelihood of paroxysmal atrial fibrillation recurrence following pulmonary vein isolation. *Circ Arrhythm Electrophysiol* 2020;.
- [10] Roney CH, Sim I, Yu J, Beach M, et al. Predicting atrial fibrillation recurrence by combining population data and virtual cohorts of patient-specific left atrial models. *Circ Arrhythm Electrophysiol* 2022;.
- [11] Lim B, Kim J, Hwang M, Song JS, et al. In situ procedure for high-efficiency computational modeling of atrial fibrillation reflecting personal anatomy, fiber orientation, fibrosis, and electrophysiology. *Scientific Reports* 2020;10(1).
- [12] Deng D, Murphy MJ, Hakim JB, Franceschi WH, et al. Sensitivity of reentrant driver localization to electrophysiological parameter variability. *Chaos* 9 2017;27(9):093932.
- [13] Azzolin L, Eichenlaub M, Nagel C, Nairn D, et al. AugmentA: patient-specific augmented atrial model generation tool. *medRxiv* 2022;doi:10.1101/2022.02.13.22270835.
- [14] Plank G, Loewe A, Neic A, et al. The openCARP simulation environment for cardiac electrophysiology. *Comput Methods Programs Biomed* 2021;208:106223.
- [15] Nagel C, Espinosa CB, Gillette K, Gsell MA, et al. Comparison of propagation models and forward calculation methods on cellular, tissue and organ scale atrial electrophysiology. *IEEE Trans Biomed Eng* 2022;(4359967):1–12.
- [16] Janssen AM, Potyagaylo D, Dössel O, Oostendorp TF. Assessment of the equivalent dipole layer source model in the reconstruction of cardiac activation times on the basis of BSPMs produced by an anisotropic model of the heart. *Med Biol Eng Comput* 6 2018;56(6):1013–1025.
- [17] Azzolin L, Schuler S, Dössel O, Loewe A. A Reproducible protocol to assess arrhythmia vulnerability : pacing at the end of the effective refractory period. *Front Physiol* 2021; 12:656411.

Address for correspondence:

Patricia Martínez Díaz, Institute of Biomedical Engineering
Karlsruhe Institute of Technology (KIT)
publications@ibt.kit.edu